Journal of Sound and Vibration (2001) **247**(3), 389–406
doi:10.1006/jsvi.2000.3736, available online at http://www.idealibrary.com on IDEAL®

SOUND RADIATION FROM A PLATE INTO A POROUS MEDIUM†

A. CUMMINGS

Department of Engineering, University of Hull, Hull, East Yorkshire HU6 7RX, England.
E-mail: a.cummings@hull.ac.uk

(*Received* 6 *September* 2000)

A nearby layer of porous sound-absorbing material has previously been shown to be capable of greatly increasing the acoustic power radiated from a vibrating flat plate, and consequently of enhancing the structural damping in the plate. In this paper, a previously published model for sound radiation from a plate of infinite extent, radiating into a semi-infinite region of absorbent, is extended to allow for a finite air gap between absorbent and plate, as well as a finite absorbent thickness. Limited parametric studies are presented here for typical cases, and model predictions are compared to finite-plate predictions and to measured data. It is concluded that the infinite-plate model can be a useful design tool, presenting minimal computational demands.

1. INTRODUCTION

The proximity of dissipative media such as porous materials can enormously increase the acoustic power radiated by vibrating solid structures such as plates. Since most of the radiated sound energy is dissipated in the absorbing medium, the net effect is of enhanced structural damping by radiation and absorption. Such damping effects are implicit in many practical applications, in particular sound insulation by double wall structures containing absorbent in the intermediate space, for example walls in buildings and aircraft fuselage structures. Free porous layers can, however, be used on their own specifically for the purpose of structural damping and noise reduction.

A previous study [1] focussed attention on the structural damping introduced, in a finite baffled plate with simply supported edges, by a layer of porous material. Two methods of analysis were presented, the first being a modal formulation for a finite thickness of absorbent separated from the plate by an air space, and the second a radiation model involving a semi-infinite region of absorbent, again placed at a given distance from the plate. Predicted and measured data were compared and generally good agreement was noted. The distribution of sound-power dissipation per unit volume in the porous medium was computed for low-frequency plate modes in the case of a zero-thickness space between plate and absorbent, as was the radiated normal intensity distribution from the plate, and some interesting effects were noted. First, the power dissipation in the absorbent was shown to be quite localized, being concentrated near the plate surface. Secondly, the radiated intensity pattern on the plate surface bore a strong resemblance to the surface displacement amplitude pattern, indicating a much more even distribution of radiation resistance than

†Some of the material in this paper was presented at the Euro-Noise 2001 meeting in Patras, Greece, 14–17 January 2001.

0022-460X/01/430389 + 18 $35.00/0

one would expect from the "corner mode" which would have existed in the case of the plate radiating into air. Indeed, this behaviour was more akin to that of a "surface mode" that would exist at frequencies greater than the critical frequency of wave coincidence for the plate. The presence of the absorbent transformed the radiation behaviour of corner modes into something more closely resembling that of surface modes, but at a sub-critical frequency. Of course, the radiation efficiency was greatly enhanced too, and a local "gas-pumping" mechanism was held to be responsible for the high sound-power losses.

Both the models reported in reference [1] are complex and require considerable effort to implement in the form of a computer code. A later study by Craik *et al.* [2], carried out in connection with the modelling of sound transmission through cavity walls with a porous interlayer, showed that the infinite-plate theory could yield surprisingly accurate results for the damping of plates radiating into porous media, even at frequencies far below the critical frequency of the plate. The theoretical result for the case studied—a semi-infinite layer of absorbent with no airspace between plate and absorbent—is very simple and can readily be implemented, either by the diligent use of a pocket calculator or by means of a short computer program.

The present study is complementary to that reported in reference [2] but deals with the more general case of a finite thickness of porous sound-absorbing material (treated as an equivalent fluid and therefore having a rigid solid frame), of infinite extent in its plane and placed at a finite distance from an infinite vibrating thin plate. The purpose of this investigation is to investigate the accuracy of the infinite-plate approach over the frequency range of interest and to highlight relevant physical phenomena. Comparisons are made between predictions based on this model and a limited range of measured data, and to predictions made by the use of the radiation model reported by Cummings *et al.* in reference [1]. In order to focus the discussion on the topic of acoustic radiation, the radiation efficiency rather than the structural damping is used as the quantity of primary interest.

2. THEORY OF SOUND RADIATION BY AN INFINITE PLATE IN THE PROXIMITY OF A LAYER OF DISSIPATIVE MATERIAL

In this section, it will be assumed that the radiating plate and the sound-absorbing layer are each of infinite extent in both directions in their planes, and that the plate carries *freely propagating* simple-harmonic bending waves of radian frequency ω as if it were *in vacuo*. These structural waves will be assumed to be one dimensional, and to consist of a standing-wave pattern as depicted in Figure 1. There is no loss in generality—for the present purposes—implicit in this assumption. Free-wave motion corresponds to resonant structural modes in a finite plate with no radiation loading, and so would only approximately represent the present case where the layer of sound-absorbing material would influence the resonant frequencies to some extent. In a practical situation, it is also possible that the plate could be excited by an incident sound field—for example, plane waves incident at a particular angle—or by direct structural excitation. In both these cases, the free-wave assumption might not be appropriate. However, it is not possible to cater for all possible types of excitation in the present discussion, and this assumption is sufficiently good for illustrative purposes.

The infinite-plate assumption renders the analysis much simpler than it would be in the case of a finite plate, though some features of the radiation at frequencies below the critical frequency f_c are lost. In particular, if the plate were radiating into a non-dissipative medium such as air below f_c, the "edge mode" and "corner mode" phenomena—wherein incomplete phase cancellation between adjacent phase cells occurs along opposite edges or at the

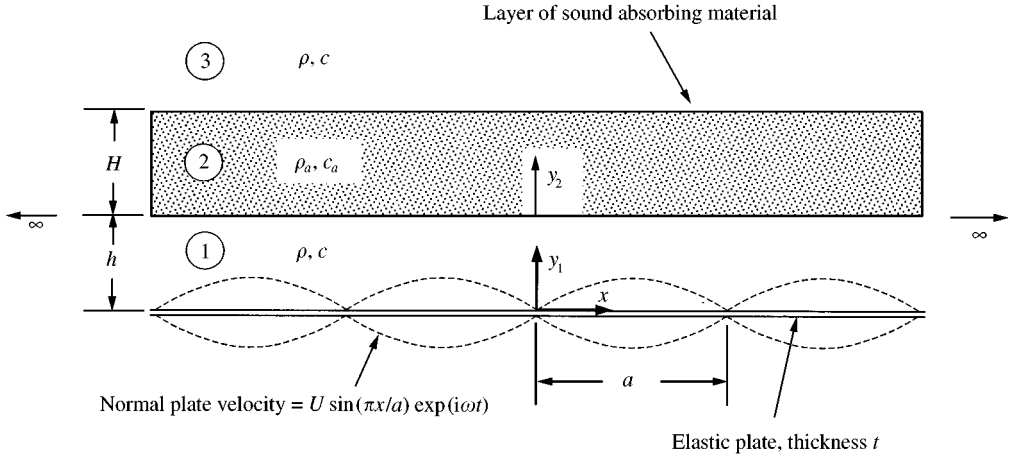

Figure 1. Two-dimensional vibrating plate with nearby sound-absorbing layer.

corners of the plate—are absent if the plate is assumed to be infinite. Edge mode radiation is generally much less efficient than "surface mode" radiation, occurring above f_c, and corner modes are even less efficient radiators, but if the plate is assumed to be infinite, theory predicts no sound power radiation at all from the plate at frequencies below f_c for *in vacuo* free structural waves. Clearly, the infinite-plate model is of no value in predicting sound radiation into a non-dissipative medium from structural modes at their *in vacuo* resonant frequencies below f_c. However, the proximity of a dissipative medium in the infinite-plate model brings about the forecast of finite radiated sound power below f_c, when what would otherwise be a purely reactive acoustic near field develops a resistive component. In this case, as discussed by Craik *et al.* [2], it is possible for the infinite-plate model to yield reasonably accurate predictions of radiated sound power and the associated radiation damping.

2.1. SOUND FIELD AND RADIATION EFFICIENCY

Since it is the radiation efficiency that is of primary concern here, the result will be identical whether we consider a single structural simple-harmonic travelling wave, a one-dimensional standing wave as shown in Figure 1 or a two-dimensional standing-wave pattern representing *in vacuo* resonant modes on a plate whose in-plane dimensions tend to infinity. The plate thickness will be denoted as t, the mass/unit area m, Young's modulus and the Poisson ratio of the plate material E and v respectively, the flexural rigidity of the plate D and the *in vacuo* free flexural wavenumber k_b. One then has

$$D = Et^3/12(1 - v^2); \quad k_b \equiv k_x = \pi/a = \omega^{1/2}(m/D)^{1/4}, \tag{1a, b}$$

where a is the width of a phase cell in the structural standing-wave pattern. The sound fields in regions 1 and 3 in Figure 1 have the governing wave equations

$$(\nabla_{xy}^2 + k^2)p_{1,3} = 0, \tag{2}$$

where ∇_{xy}^2 is the two-dimensional Laplacian operator and $k = \omega/c$, c being the sound speed. Solutions to equation (2) yield expressions for the y-wavenumbers,

$$k_{y1,3} = \sqrt{k^2 - (\pi/a)^2}. \tag{3}$$

For $f < f_c$, these wavenumbers are imaginary. In region 2, the porous material is characterized by two "equivalent fluid" complex, frequency-dependent parameters, for example, the effective density ρ_a and the equivalent sound speed c_a (see Figure 1). The governing wave equation here is

$$(\nabla_{xy}^2 + k_a^2)p_2 = 0, \tag{4}$$

where $k_a = \omega/c_a$. The y-wavenumber in region 2 is now given by

$$k_{y2} = \sqrt{k_a^2 - (\pi/a)^2}. \tag{5}$$

Solutions for the sound-pressure fields in regions 1, 2 and 3 must (as may be shown by matching the plate velocity to the particle velocity in region 1 and the sound pressures or particle velocities across the interfaces at either side of the porous layer) contain the factor $\sin(\pi x/a)$. Appropriate expressions for these solutions are then

$$p_1(x, y; t) = e^{i\omega t}\sin(\pi x/a)(Ae^{-ik_{y1}y_1} + Be^{ik_{y1}y_1}), \tag{6a}$$

$$p_2(x, y; t) = e^{i\omega t}\sin(\pi x/a)(Ce^{-ik_{y2}y_2} + De^{ik_{y2}y_2}), \tag{6b}$$

$$p_3(x, y; t) = e^{i\omega t}\sin(\pi x/a)Ee^{-ik_{y1}y_2}. \tag{6c}$$

In equations (6a–c), A–E are arbitrary, complex, constants. In equation (6c), a purely outgoing wave solution has been taken, since it is assumed that there are no wave reflections in region 3 from the positive y_2 direction, and $k_{y1} = k_{y3}$ is also used. Implementation of the boundary conditions of continuity of sound pressure and normal particle velocity at $y_2 = H$ yield, *via* the use of the acoustic Euler equation $u_y = -(1/i\omega\rho)\partial p/\partial y$ (u_y being normal particle velocity and ρ being air density, or effective density in the case of the porous layer),

$$D/C = \exp(-i2k_{y2}H)(k_{y2}\rho/k_{y1}\rho_a - 1)/(k_{y2}\rho/k_{y1}\rho_a + 1). \tag{7}$$

A similar procedure, applied at $y_2 = 0$, $y_1 = h$, yields

$$A/C = (1/2)\exp(ik_{y1}h)[(k_{y2}\rho/k_{y1}\rho_a + 1) - \exp(-i2k_{y2}H)(k_{y2}\rho/k_{y1}\rho_a - 1)^2/(k_{y2}\rho/k_{y1}\rho_a + 1)], \tag{8a}$$

$$B/C = -(1/2)\exp(-ik_{y1}h)(k_{y2}\rho/k_{y1}\rho_a - 1)[1 - \exp(-i2k_{y2}H)] \tag{8b}$$

and

$$B/A = -\exp(-i2k_{y1}h)[1 - \exp(-i2k_{y2}H)]/[(k_{y2}\rho/k_{y1}\rho_a + 1)/(k_{y2}\rho/k_{y1}\rho_a - 1) - \exp(-i2k_{y2}H)(k_{y2}\rho/k_{y1}\rho_a - 1)/(k_{y2}\rho/k_{y1}\rho_a + 1)]. \tag{8c}$$

Finally, matching the particle velocity in the sound field in region 1 to the plate velocity at $y_1 = 0$ gives

$$A = (\omega\rho U/k_{y1})/(1 - B/A). \tag{8d}$$

The normal component of the acoustic intensity radiated by the plate into region 1 is given by

$$I_y^{(1)}(x) = \overline{\mathrm{Re}(p_1|_{y_1=0})\mathrm{Re}(u_p)}, \tag{9}$$

where u_p is the plate velocity,

$$u_p = U \sin(\pi x/a) \exp(\mathrm{i}\omega t) \tag{10}$$

(see Figure 1). Equations (6a) and (10) may be inserted into equation (9) to yield an expression for the space-averaged intensity component in the y direction,

$$\langle I_y^{(1)}(x) \rangle = \rho\omega U^2 \mathrm{Re}[F(\omega)]/4 \tag{11}$$

(the angle brackets denoting a space average), where

$$F(\omega) = (1/k_{y1})(1 + B/A)/(1 - B/\mathrm{A}). \tag{12}$$

The ratio B/A is found from equation (8c). The radiation efficiency σ of the plate is then given by

$$\sigma = \langle I_y^{(1)}(x) \rangle / (\rho c \langle \overline{|u_p|^2} \rangle / 2) = k \ \mathrm{Re}[F(\omega)]. \tag{13}$$

This expression for radiation efficiency is the same, whether a one-dimensional or two-dimensional standing-wave pattern is assumed for the plate displacement. It becomes identical to the expression given by Craik *et al.* [2] if $h \to 0$ and $H \to \infty$.

2.2. INSERTION LOSS OF POROUS LAYER

It is of interest also to determine the acoustic insertion loss (IL) of the porous layer, while assuming the plate velocity is unaffected by the presence of the absorbent. This assumption would not necessarily be valid in practice, but the effect of the absorbent of the motion of the plate would depend on the way in which the plate were excited, and it is not possible to account for this in a general way. Because an infinite plate with no absorbent layer carrying free bending waves will radiate no acoustic power below f_c, it is only possible to define the IL for $f > f_c$. The y component of intensity in region 3 is

$$I_y^{(3)}(x) = \overline{\mathrm{Re}(p_3|_{y_2 = H}) \, \mathrm{Re}(u_{y3}|_{y_2 = H})}, \tag{14}$$

where u_{y3} is the y component of the particle velocity in region 3. If one defines a function

$$G(\omega) = (E/C)/[k_{y1}(1 - B/A)A/C], \tag{15}$$

then it may be shown that

$$\langle I_y^{(3)}(x) \rangle = (\rho\omega U^2/4) k_{y1} |G(\omega)|^2. \tag{16}$$

An "external" radiation efficiency may be defined, and expressed as

$$\sigma_e = \langle I_y^{(3)}(x) \rangle / (\rho c \langle \overline{|u_p|^2} \rangle / 2) = k k_{y1} \ |G(\omega)|^2. \tag{17}$$

This quantity relates the space-averaged intensity radiated from the absorbing layer into region 3 to that radiated at an infinitely high frequency from the panel alone into air. In the absence of an absorbing layer, the radiation efficiency of the panel is

$$\sigma_0 = 1/\sqrt{1 - (\pi/ka)^2}, \tag{18}$$

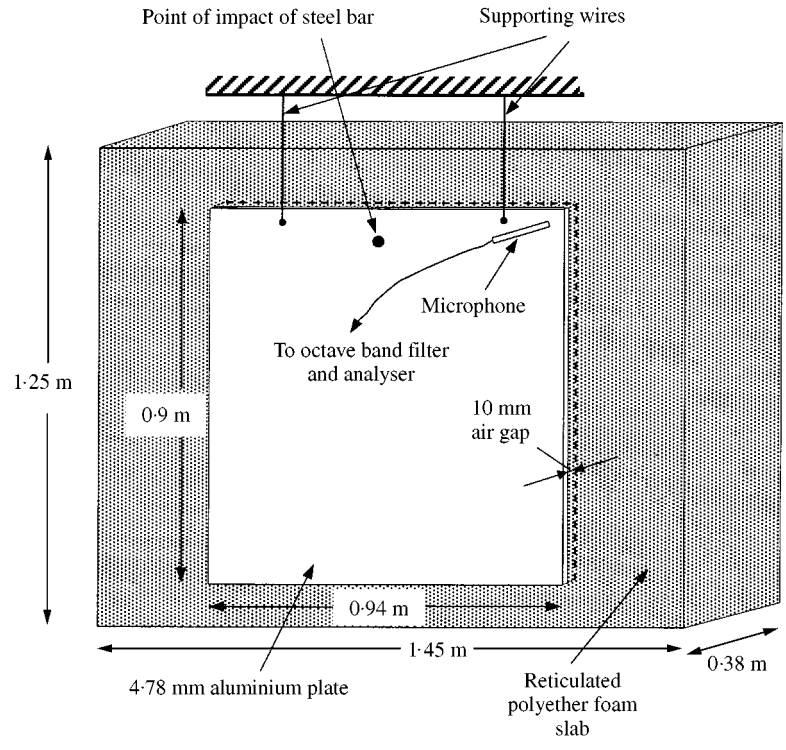

Figure 2. Experimental apparatus with suspended plate.

provided $f > f_c$. Clearly, one has

$$IL = 10\log(\sigma_0/\sigma_e) = -20\log[k_{y1}|G(\omega)|], \tag{19}$$

since k_{y1} is real for $f > f_c$.

3. EXPERIMENTS

For the purposes of comparison between predicted and measured data, a limited set of experiments was carried out in the present investigation. (Other experimental results from the paper by Cummings *et al.* [1]—the method of obtaining which is described in that paper—are also used here.) The arrangement is shown in Figure 2. A block of reticulated polyether foam, measuring 1·25 m × 1·45 m × 0·38 m, was placed on the laboratory floor, resting on one of its 1·45 m × 0·38 m sides. This foam block was actually that used in the experiments reported by Cummings *et al.* [1]; its steady flow resistivity was 6992 mks rayl/m and its other "equivalent fluid" parameters are described in reference [1]. The curve-fitting method of Delany and Bazley [3] was used to predict its frequency-dependent bulk properties and at low frequencies—where this method fails—the formulae proposed by Mechel [4] were employed. An aluminium plate measuring 0·9 m × 0·94 m × 4·78 mm was suspended by two steel wires, so that it was 10 mm from one vertical surface of the slab of foam. The plate was deliberately mounted in this way, so that its boundary conditions were "non-standard", in an effort to test the accuracy of the infinite-plate predictions in a case where the edge mounting conditions would not be readily specified in simple terms.

Furthermore, the plate was not mounted in a baffle. In practical cases, radiating structures would not normally be baffled, and neither would their structural boundary conditions be straightforward. To this extent, an attempt was made to avoid idealized test mounting conditions, if not to simulate a typical practical situation.

The plate was excited over a broad frequency range by striking it with the end of a steel bar, towards its upper edge. The impact was not such as to cause the plate to move significantly. The vibratory motion of the plate was detected by means of a microphone placed a few millimeters from the plate surface near a corner, so that it would respond to the near-field sound pressure. Because the edges of the plate were unsupported, all its vibrational modes should have a velocity maximum at a corner. The microphone output was passed through an octave band filter and fed to an analyzer. The reverberant decay of the plate was thus recorded in octave bands. From elementary theory, it is readily shown that if the plate radiates only from *one* side, then its radiation efficiency is given by

$$\sigma = 13{\cdot}82m/\rho ct_R, \tag{20a}$$

where m is (as before) the mass/unit area of the plate and t_R is the time taken for the reverberant vibration level of the plate to decay by 60 dB. Thus, for $f < f_c$, where sound radiation from the side of the plate remote from the polyether foam slab should be negligibly small, equation (20a) gives the experimental value of σ. For $f > f_c$, however, radiation from that side of the plate cannot be ignored, and one has

$$\sigma = 13{\cdot}82\, m/\rho ct_R - \sigma_0, \tag{20b}$$

where σ_0 is given by equation (18). The critical frequency of the plate used in the tests was 2486 Hz, and in all frequency bands up to and including the 2 kHz band, equation (20a) was used to find σ. Above 2 kHz, equation (20b) was employed. Because of the difficulty in applying equation (18) in the band containing f_c, the radiation efficiency in this band was left uncorrected.

The frequency range of the measurements was 63 Hz–8 kHz. Regression lines were fitted to the time decay in the vibrational level of the plate, and fairly linear decay plots were obtained, especially at the higher frequencies.

4. PREDICTED AND MEASURED RESULTS

In this section, comparison is made between the radiation efficiency predicted by the infinite-plate theory described here and that predicted by the "radiation model" for sound radiation from a finite plate, reported by Cummings *et al.* [1]. A range of predictions based on the infinite-plate model is also presented in an effort to illustrate the physical processes involved. Comparison is made between infinite-plate predictions and measurements of σ made as described in section 3, and between finite-plate predictions, measurements taken from reference [1] and infinite-plate predictions.

4.1. FINITE-PLATE *VERSUS* INFINITE-PLATE PREDICTIONS

In Figure 3(a) is shown a comparison between the computed radiation efficiency of a 3 mm thick aluminium plate—measuring 1 m × 0·8 m and located 5 mm away from a semi-infinite thickness of fibrous material having a steady flow resistivity of 2×10^4 mks rayl/m—based both on the infinite-plate model described here and on the

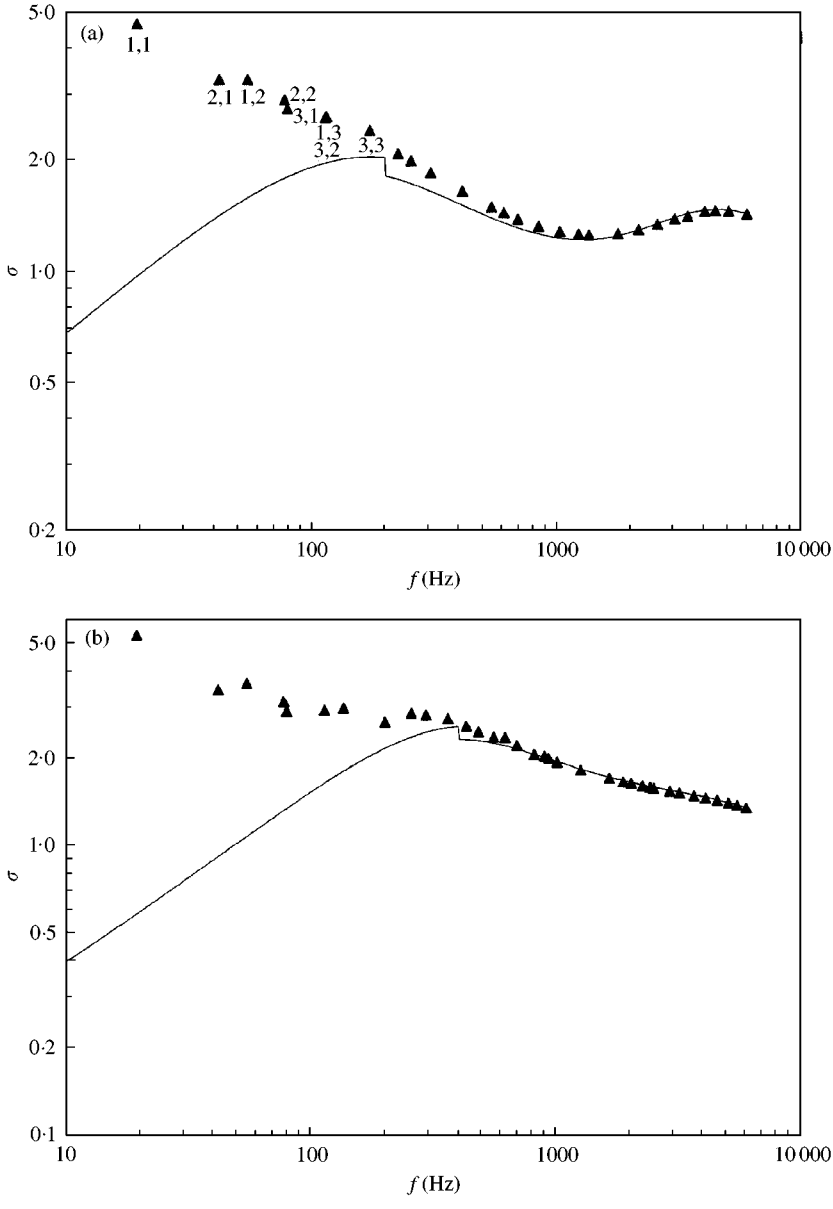

Figure 3. Predicted radiation efficiency of simply supported $1\,m \times 0{\cdot}8\,m$ aluminium plate, $t = 3$ mm, $h = 5$ mm, $H = \infty$. Fibrous absorbent; (a) steady flow resistivity 2×10^4 mks rayl/m, (b) steady flow resistivity 4×10^4 mks rayl/m. ——, infinite-plate theory; ▲, finite-plate theory (radiation model) [1].

finite-plate radiation model of reference [1]. The plate has a critical frequency of 3960 Hz. The data of Delany and Bazley [3] and the low-frequency model of Mechel [4] were used to predict the bulk acoustic properties of fibrous media in this investigation. In the case of the finite-plate model, σ is computed for individual plate modes at their *in vacuo* resonant frequencies. All modes up to the (3,2) mode are plotted, and at higher frequencies only selected modes are shown. The mode numbers are shown for modes up to the (3,3) mode. Gaussian quadrature was used to compute the quadruple integral required to find the

sound power radiated from the plate, and it proved necessary to employ 10- and 12-point quadratures here, in place of the 5- and 6-point quadratures used for the computations reported in reference [1]. Otherwise the computational methods were similar. More accurate integration was needed here largely because of the higher upper-frequency limit of the present calculations. The amplitude of the sound-pressure field radiated along the plate surface, by a point source element, falls much more rapidly at high frequencies than at low frequencies, because of the greater attenuation coefficient in the porous material. A greater number of points was therefore required in the integration scheme to resolve this more rapid decay.

It can be seen that the radiation efficiencies predicted by the finite and infinite-plate models agree very well above about 200 Hz, and a broad peak in σ around f_c is evident. (The jump in predicted values at 200 Hz is unimportant, being caused by modest discrepancies between the Mechel and Delany and Bazley methods for predicting the bulk acoustic properties of the absorbent.) Below 200 Hz, the finite-plate model predicts greater values of σ than those from the infinite-plate model, with the discrepancies increasing as the frequency falls. For the fundamental plate mode, the finite-plate model predicts the radiation efficiency to be almost 5 times that forecast by the infinite-plate model. A physical mechanism for this difference between the two models at low frequencies may be offered, as follows. Because there is an air gap between the plate and the absorbent, partial phase cancellation can occur between the sound radiation from adjacent phase cells of opposite sign on the plate surface. In the finite-plate model, however, rectangular areas at the corners or edges of the plate do not undergo this cancellation process and radiate significant acoustic power into the air gap, where it is absorbed by the porous material. In the infinite-plate model, partial phase cancellation occurs over the entire plate area and so less radiated sound power is predicted. As the frequency rises, the orders of the resonant modes in the finite plate increase. If no absorbent were present, this effect would, to some extent, offset the increase in modal radiation efficiency brought about by increasing frequency, because of the reduced radiating area at the plate corners or edges with increasing mode order. However, with a layer of absorbent placed close to the plate surface, the higher the mode order, the less effectively do the corners or edges radiate into the air gap because the advantageous multipole frequency effect is inhibited by dissipation in the absorbent. Eventually, corner- and edge-mode radiations tend to give way to the dissipative mechanism that occurs in the central part of the plate. (The "edge mode" and "corner mode" terminology is used rather loosely here where a dissipative layer is present, since these terms only apply properly where the plate radiates into air.) At frequencies above this point, the finite-plate and infinite-plate theories will give very similar predictions. In the case of the infinite plate, the presence of the absorbent renders what would otherwise be a reactive near field, radiating no energy, partially resistive so that energy "leaks" into the absorbent. Above the critical frequency of the plate, the absorbent tends to have less effect on the radiation efficiency and—apart from the fact that the sharp peak in σ where $f = f_c$ is absent when absorbent is present—there is no dramatic difference between the cases with and without absorbing material.

In Figure 3(b) are shown computed radiation efficiency data for the aluminium plate of Figure 3(a), but with a fibrous absorbent having a steady flow resistivity of 4×10^4 mks rayl/m. The comparison between the finite-plate and infinite-plate predictions is very similar to that in Figure 3(a) but the broad peak in σ close to the critical frequency, evident in the case of the lower-flow-resistivity absorbent, is absent here. The greater dissipative capacity of this higher-flow-resistivity material is likely to be the cause of this effect. Also, the finite and infinite-plate predictions begin to diverge at about 400 Hz, as compared to 200 Hz in the case of the data in Figure 3(a). This would be expected on the basis of the

foregoing arguments since, in the case of an absorbent with a higher flow resistivity, a higher frequency would have to be reached before the same degree of "dissipative coupling" could be achieved between the near field of the plate and the absorbent. The degree of impedance mismatch between air and the absorbent falls as the numerical value of frequency ÷ flow resistivity rises. Since the dissipative coupling is likely to be stronger for a lesser degree of impedance mismatch, frequency and flow resistivity tend to act in opposition in this regard.

The above arguments are based on the assumption that there is an air gap and that it is fairly small. As the air gap between the plate and absorbent narrows, the onset of predominance of the near-field leakage effect moves to progressively lower frequencies, and corner- and edge-mode radiations become suppressed to an increasing extent. Finally, for a zero air gap, a finite plate behaves very much like an infinite plate, at least for absorbents of moderate steady flow resistivity. In Figure 4(a, b) are shown two cases, for steady flow resistivities of 10^4 and 4×10^4 mks rayl/m respectively. It can be seen that the finite- and infinite-plate predictions agree well over the entire frequency range. The small discrepancies are probably caused by numerical errors in the finite-plate computations, which involve the use of several numerical techniques. It is clear that, for vanishingly small air gaps, the infinite-plate formulation is an excellent substitute for the much more computationally demanding finite-plate theory.

4.2. INFINITE PLATES: THE EFFECTS OF AIR GAP AND ABSORBENT THICKNESS

It is of interest to examine the dependence of σ on h and H. In Figure 5, a family of curves is shown for $H = \infty$ and a range of values of h from 0 to 200 mm, for an infinite 3-mm-thick aluminium plate with a fibrous absorbent. At low to mid frequencies, a progressive fall in σ is predicted as h increases, while for $f > 6$ kHz, σ is almost independent of h. The importance of the air gap being small is well illustrated, though there is very little difference in σ above about 60 Hz between the cases of $h = 0$ and 2 mm. Although generally small values of radiation efficiency are predicted for $h > 20$ mm and $f < 2$ kHz, the results and discussion of section 4.1 indicate that the actual values of σ would be significantly higher, especially at low frequencies, because of corner- and edge-mode radiations. Oscillations in σ are predicted in the curve with $h = 200$ mm for $f > f_c$, because of damped standing-wave effects between the plate and the absorbing layer. One also notes that the predictions for $h \leqslant 2$ mm are likely to be reasonably accurate above about 60 Hz.

The fall-off in σ with increasing h below 2 kHz may be explained by the rapid spatial decay (the $\exp(-ik_{y1}y)$ factor in equation (6a)) in the outgoing wave amplitude, away from the plate surface, occurring because $f < f_c$ and k_{y1} is imaginary. The porous layer increases σ by energy dissipation because of the aforementioned resistive leakage effect from what would otherwise be a reactive near field of the plate. But the farther the absorbing layer is from the plate, the smaller this increase is. One should note that the particle velocity generally has a significant component parallel to the plate surface. In the absence of the absorbing layer, for $f < f_c$, it is readily shown from equation (6a) that

$$u_y/u_x = \tan\theta = -\sqrt{1-(ka/\pi)^2}\,\tan(\pi x/a), \tag{21}$$

where u_x, u_y are the x and y components of particle velocity in the outgoing wave field and θ is the slope of the acoustic streamlines. If one puts $\theta = \mathrm{d}y/\mathrm{d}x$ and integrates (21), an equation for the acoustic streamlines results,

$$y/a = (1/\pi)\sqrt{1-(ka/\pi)^2}\ln|\cos(\pi x/a)/\cos(\pi x_0/a)|, \tag{22}$$

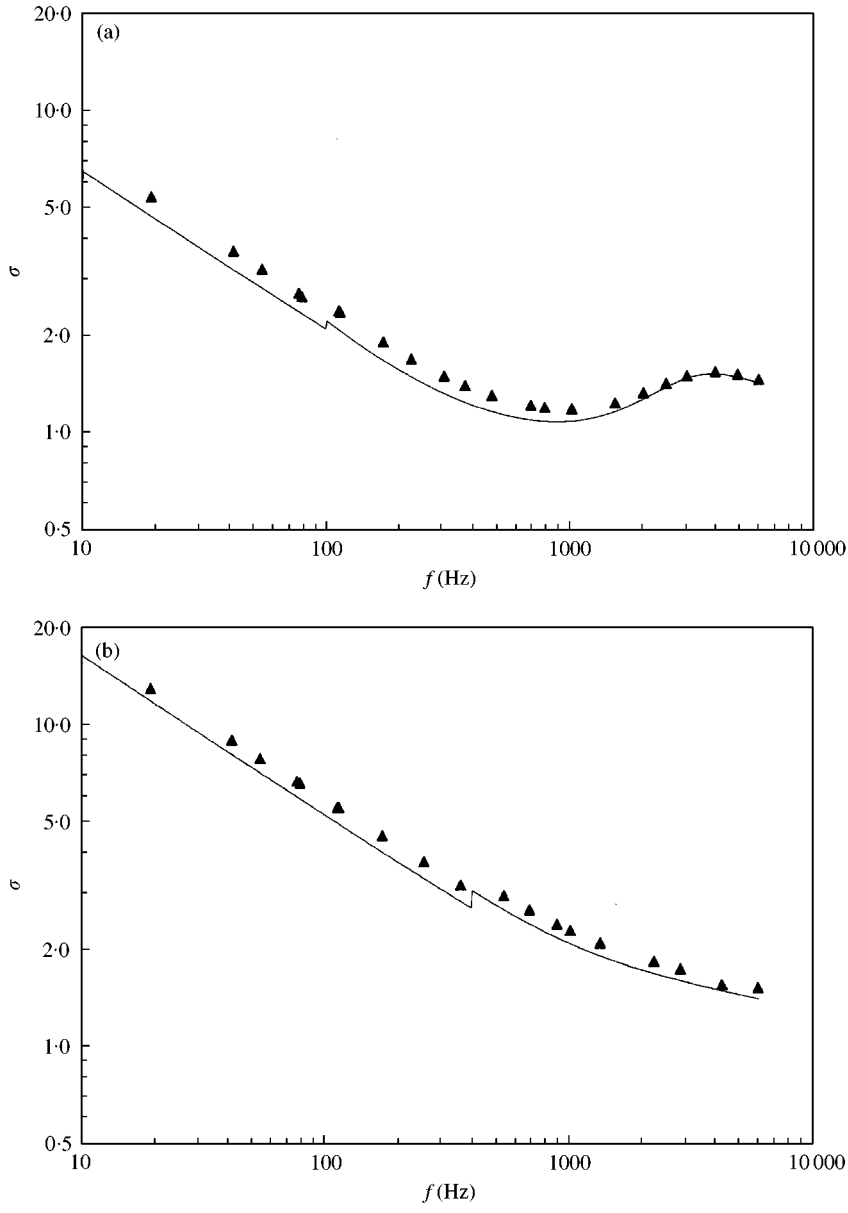

Figure 4. Predicted radiation efficiency of simply supported $1\,\text{m} \times 0{\cdot}8\,\text{m}$ aluminium plate, $t = 3$ mm, $h = 0$, $H = \infty$. Fibrous absorbent; (a) steady flow resistivity 10^4 mks rayl/m, (b) steady flow resistivity 4×10^4 mks rayl/m. ——, infinite-plate theory; ▲, finite-plate theory (radiation model) [1].

where x_0 is one or the other of the points at which a particular streamline meets the plate surface. Equation (22) may be plotted for various values of x_0, to give an indication of the acoustic streamline pattern. An example of such a pattern is shown in Figure 6, for $ka = 0{\cdot}01$. The plate vibration pattern is shown, with positive and negative phase cells indicated. It should be noted that the particle velocity amplitude decays rapidly away from the plate, in the y direction. Over most of the frequency range below f_c, the particle motion is essentially confined to a region near the plate surface, where the motion is predominantly

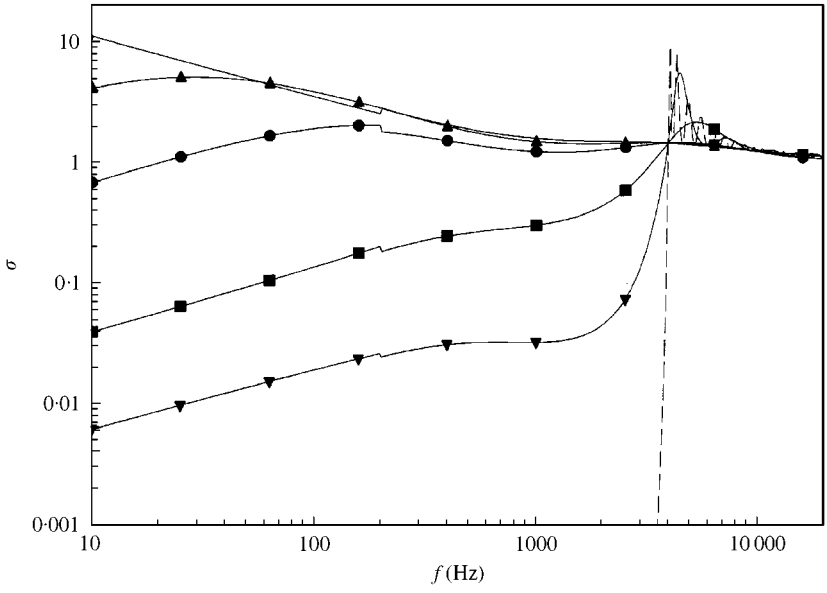

Figure 5. Predicted radiation efficiency of infinite aluminium plate, $t = 3$ mm, $H = \infty$, for various values of h. Fibrous absorbent material, steady flow resistivity $= 2 \times 10^4$ mks rayl/m. ——, $h = 0$; ▲——▲, $h = 2$ mm; ●——●, $h = 5$ mm; ■——■, $h = 20$ mm; ▼——▼, $h = 50$ mm; — — — —, $h = 200$ mm.

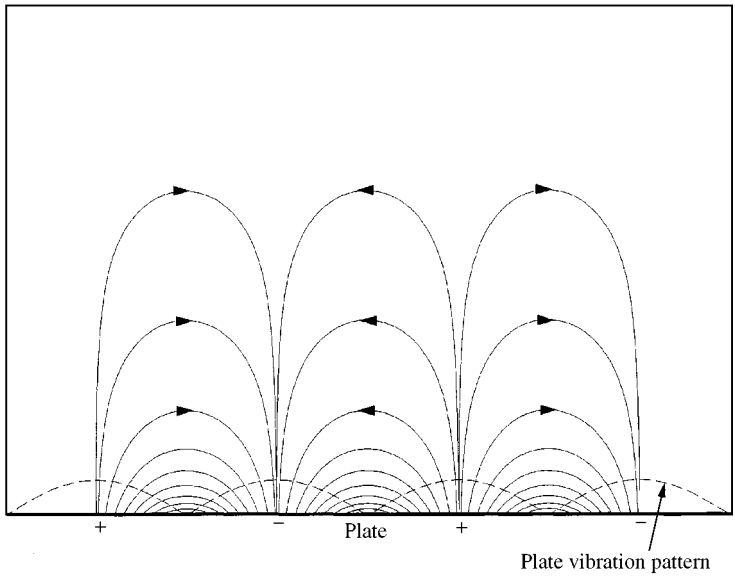

Figure 6. Acoustic streamlines in the reactive near field of a vibrating plate (with no nearby absorbent layer) below the critical frequency; $ka = 0{\cdot}01$.

transverse. Equation (22) indicates that, as f_c is approached and ka/π rises, the streamline pattern simply becomes "squashed up" toward the plate as the square root factor decreases in value.

The effects of changing the thickness of the absorbent layer are shown in Figure 7, for the 4·78 mm plate used in the experiments described in section 3, with the same polyether foam

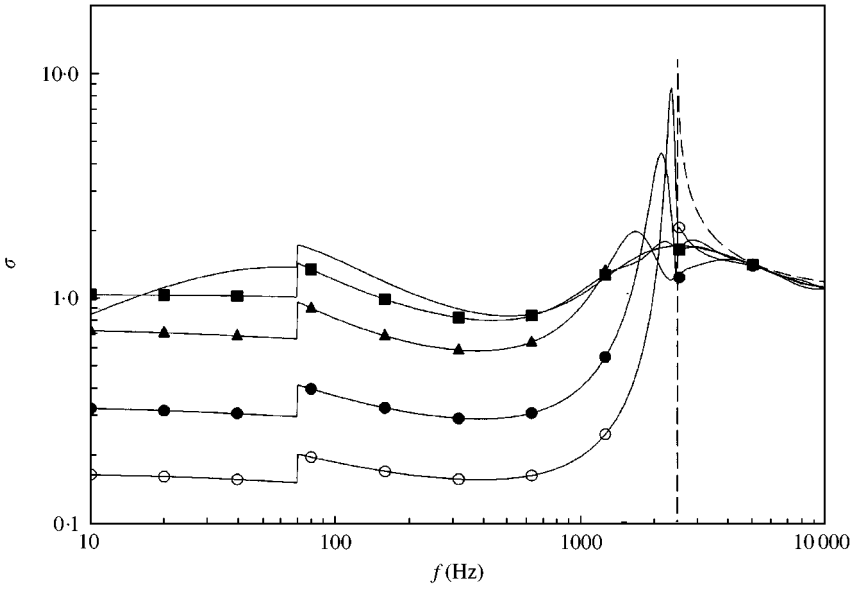

Figure 7. Predicted radiation efficiency of infinite aluminium plate, $t = 4{\cdot}78$ mm, $h = 10$ mm, for various values of H. Polyether foam absorbent, steady flow resistivity 6992 mks rayl/m. – – – – –, $H = 0$; ○——○, $H = 10$ mm; ●——●, $H = 20$ mm; ▲——▲, $H = 50$ mm; ■——■, $H = 100$ mm; ——, $H = \infty$.

placed 10 mm from the plate. As one would expect, a semi-infinite thickness of absorbent gives the highest radiation efficiency overall, with a progressive decrease in σ as H decreases. It can be seen, however, that a 100 mm absorbent thickness gives radiation efficiencies almost as high as a semi-infinite thickness. Therefore, at least from the point of view of plate damping, there would be no need to place large thicknesses of absorbent near the plate in order to achieve the maximum radiation-damping effect.

4.3. INSERTION LOSS OF THE ABSORBENT LAYER

Although—as mentioned in section 2—the IL of the absorbent layer is only defined in the infinite-plate model for $f > f_c$, it is still worth computing the IL for some typical situations. The IL, predicted from equation (19) for various thickness layers of the polyether foam used in the experiments described here, is shown in Figure 8; the plate is of 4·78 mm aluminium and the air gap is 10 mm wide. For all absorbent thicknesses, the IL rises sharply as the frequency approaches f_c from above. As one would expect, the IL generally increases as H increases, and is roughly proportional to H for $f > 2f_c$, consistent with the IL mechanism arising principally from travelling-wave absorption in the bulk material. This seems reasonable when one considers that wave reflection at the air/absorbent interfaces will be quite minor at these high frequencies, where the characteristic impedance of the absorbent is not too far removed from the characteristic impedance of air. Quite high insertion losses, of 16–17 dB, are achieved for a 100 mm absorbent thickness above about 3 kHz.

In Figure 9, the IL of a 50 mm layer of polyether foam, placed at various distances from a 4·78 mm aluminium plate, is shown. Changing h evidently makes little difference to the IL, although some damped resonance effects appear as f_c is approached from above for

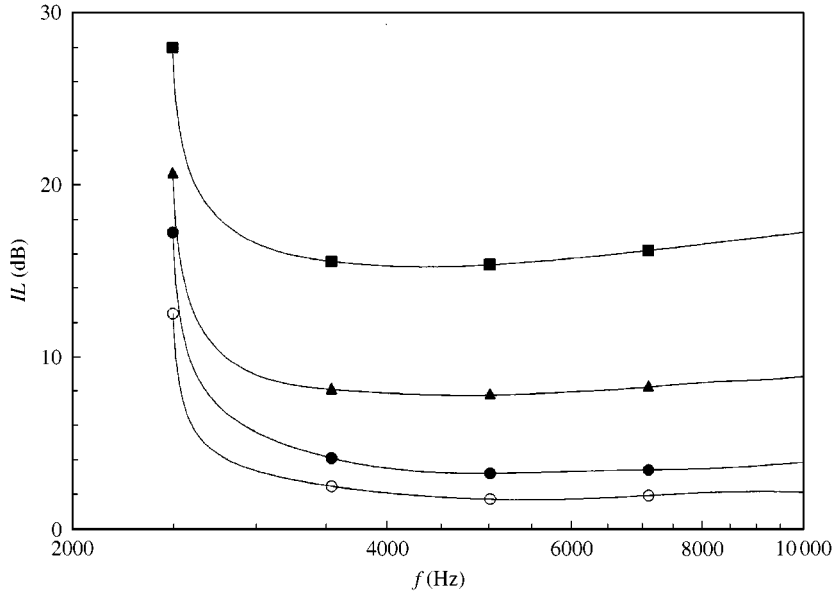

Figure 8. Predicted insertion loss of various thicknesses of polyether foam (steady flow resistivity 6992 mks rayl/m) placed 10 mm from an infinite aluminium plate, $t = 4{\cdot}78$ mm. ■——■, $H = 100$ mm; ▲——▲, $H = 50$ mm; ●——●, $H = 20$ mm; ○——○, $H = 10$ mm.

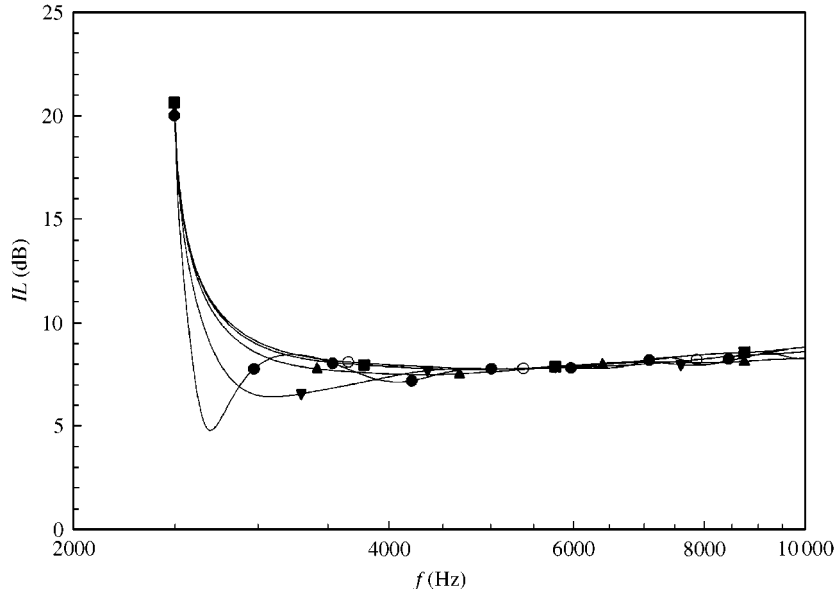

Figure 9. Predicted insertion loss of a 50 mm thickness of polyether foam (steady flow resistivity 6992 mks rayl/m) placed at various distances from an infinite aluminium plate, $t = 4{\cdot}78$ mm. ○——○, $h = 5$ mm; ■——■, $h = 10$ mm; ▲——▲, $h = 20$ mm; ▼——▼, $h = 50$ mm; ●——●, $h = 100$ mm.

$h = 100$ mm. This is presumably caused by an increasing wave reflection coefficient at the air/absorbent interfaces, brought about by the increasingly oblique angle of incidence of waves on these interfaces as f_c is approached.

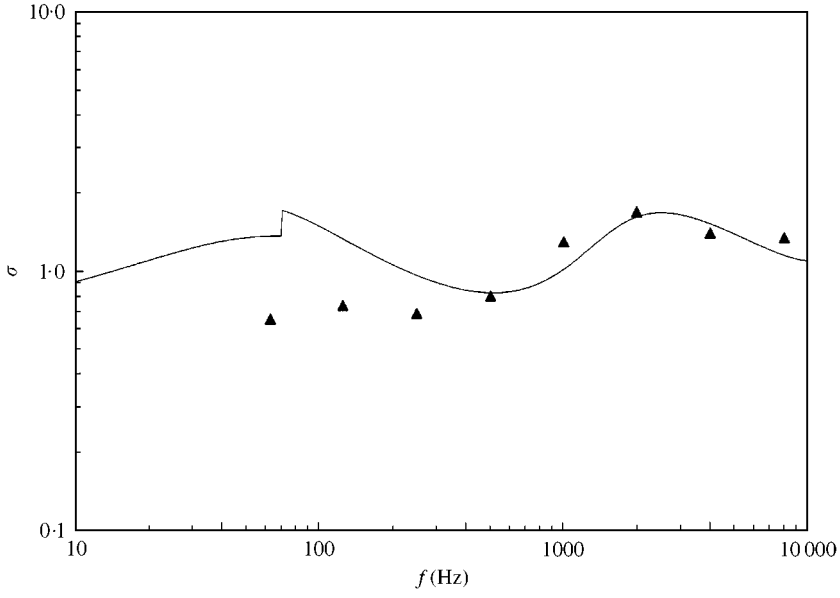

Figure 10. Predicted and measured radiation efficiency of 0·9 m × 0·94 m suspended aluminium plate, $t = 4{\cdot}78$ mm, $h = 10$ mm, $H = 0{\cdot}38$ m; polyether foam absorbent, steady flow resistivity 6992 mks rayl/m. ▲, measured data; ——, infinite-plate prediction.

Of course, as previously mentioned, it is not generally the case that the motion of the plate will be unaffected by the presence of the absorbing layer as is assumed here. It is likely that, in practical situations, the increased radiation damping will reduce the vibration amplitude of the plate, particularly near resonance frequencies. Consequently, the *IL* should attain greater values than those given by equation (19). Furthermore, it has been assumed that free structural waves are present in the (infinite) plate, the equivalent of resonant modes in a finite plate. A different structural wavefield—perhaps forced by point structural excitation or by a sound field incident from the other side of the plate—would give rise to a different behaviour of the *IL*.

4.4. COMPARISON BETWEEN PREDICTED AND MEASURED RADIATION EFFICIENCY

A comparison between the results of the experiments described in section 3 and infinite-plate prediction of the radiation efficiency is shown in Figure 10. Agreement between predictions and measurement is very close from 500 Hz to 8 kHz. From 63 Hz to 250 Hz, the infinite-plate theory over-predicts σ, to an increasingly great extent as the frequency falls. These discrepancies are not, however, dramatic and are almost certainly caused by "edge leakage" effects in corner-mode radiation. Because the plate was not mounted in a baffle, partial volume velocity cancellation would occur along its edges at the lower frequencies. Overall, the infinite-plate theory gives quite satisfactory predictions of radiation efficiency.

Some of the experimental data from the paper by Cummings *et al.* [1], for a 458 mm × 250 mm × 1 mm baffled aluminium plate with a 4·4 mm air gap and the aforementioned polyether absorbent, are plotted in the form of radiation efficiency in Figure 11 (they were originally presented as structural loss factor). Also plotted are

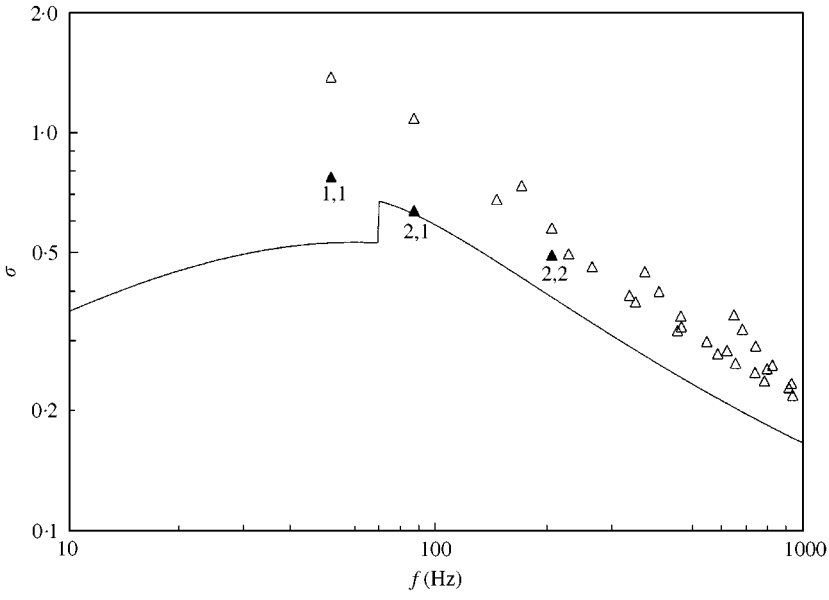

Figure 11. Predicted and measured radiation efficiency of 0·458 m × 0·25 m simply supported aluminium plate, $t = 1$ mm, $h = 4{\cdot}4$ mm, $H = 0{\cdot}38$ m; polyether foam absorbent, steady flow resistivity 6992 mks rayl/m. ▲, measured data [1]; ——, infinite-plate prediction; Δ, baffled finite-plate prediction with $H = \infty$ [1].

theoretical values of σ from the infinite-plate model described here and the baffled finite-plate radiation model of reference [1]. The finite-plate predictions all lie above the infinite-plate curve, the differences between the two prediction methods increasing as the frequency falls. The three experimental data points from reference [1] lie intermediate between the infinite-plate curve and the finite-plate predictions. Agreement between prediction and measurement is reasonable. A physical explanation for the differences between the finite- and infinite-plate predictions of σ is given in section 4.1. The fact that the infinite-plate prediction is in better agreement with the measured data that the finite-plate points is probably coincidental.

4.5. COMPARISON WITH A PLATE RADIATING INTO AIR

It is worth comparing the radiation efficiency of a typical plate radiating into air, and into a porous material, in order to give a general perspective on the problem. Sample computed data at the *in vacuo* resonant frequencies are shown in Figure 12, for a 1 m × 0·8 m × 3 mm aluminium plate. Both an infinite-plate curve and finite-plate data for modes with *in vacuo* structural resonant frequencies up to 500 Hz are shown, for the plate situated 1 mm from an infinite thickness of fibrous medium with a steady flow resistivity of 2×10^4 mks rayl/m, and also radiating into air. (Some of the mode numbers are shown for the plate radiating into air.) The air-gap thickness of 1 mm was chosen because it is about the minimum that can be realized in practice with any accuracy, and yields radiation efficiencies very close to the maximum obtainable values for the case of a zero-thickness air gap. There is good agreement between the infinite-plate and finite-plate data for the plate radiating into the fibrous medium. The values of σ range from about 1·6, at 1 kHz, to 10, at 10 Hz, and there is a monotonic fall in σ from low to high frequencies. In contrast, the modal radiation

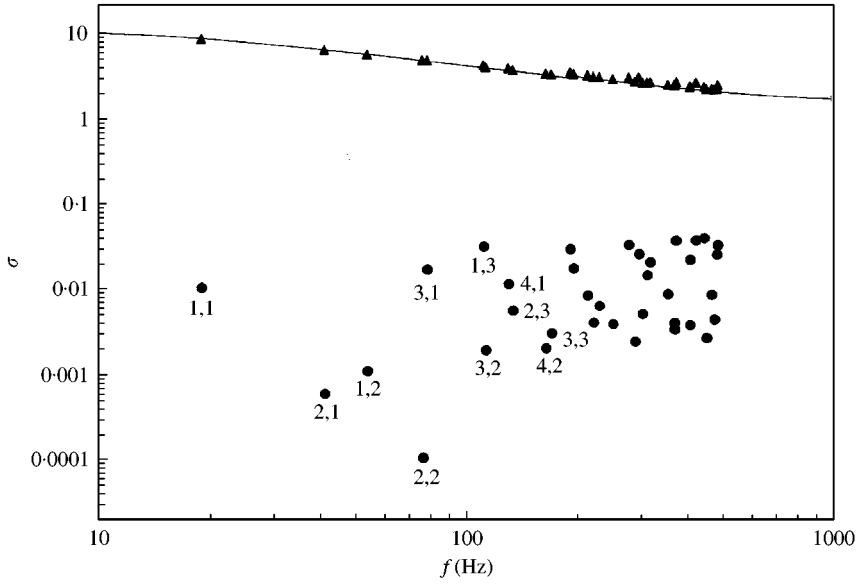

Figure 12. Predicted radiation efficiency of simply supported $1\,m \times 0{\cdot}8\,m$ aluminium plate, $t = 3$ mm, $h = 1$ mm, $H = \infty$. ———, infinite-plate theory, ▲, finite-plate theory (radiation model) [1], with fibrous absorbent, steady flow resistivity 2×10^4 mks rayl/m; ●, finite-plate theory (radiation model) [1], with plate radiating into air.

efficiencies for the plate radiating into air are very much smaller, by a factor of up to 4·5 orders of magnitude. Furthermore, these figures vary greatly, depending on the mode order as well as the frequency. As expected, the doubly "non-volume-cancelling" corner modes (e.g. (1, 1), (3, 1), (1, 3)) radiate most efficiently, while the doubly "volume-cancelling" corner modes (e.g. (2, 2), (4, 2)) are the least efficient.

The data presented in Figure 12 help to stress the main features of radiation from a plate into a dissipative medium. First, the radiation damping is enormously increased by the presence of the porous medium, and secondly there is a much smoother frequency dependence of the radiation efficiency with a nearby layer of porous material than without. Also, the radiation efficiency tends to increase as the frequency falls, which can be a distinct advantage in practical applications, where the predominant excitation might well be at low frequencies. Finally, the infinite-plate predictions are—for either a very small or zero-thickness air gap—close to the finite-plate figures, over the frequency range of interest.

5. CONCLUSIONS

An infinite-plate approximation for sound radiation from a simply supported baffled plate into a layer of a dissipative medium has been investigated here, and it has been shown to yield good results under certain conditions, as compared to measured data and finite-plate predictions. In particular, the approximation works well over the whole frequency range of interest when the air gap between the plate and layer of absorbent is very small. For larger air gaps, the method gives accurate predictions of radiation efficiency above a certain lower limiting frequency. The role of absorbent thickness has been investigated and, in the cases studied, it has been shown that a moderately thick layer of absorbent behaves as if it were effectively infinite.

A nearby layer of sound-absorbing material can greatly enhance the acoustic radiation from a vibrating plate, and can be a useful way of increasing the structural damping as well as reducing the sound radiated to the exterior region. The infinite-plate formulation presented here is a relatively simple way of predicting the acoustic radiation efficiency and consequent structural damping, and could be used in a predictive design scheme for noise control. It requires little in the way of computational effort.

It has been assumed here—as in previous studies [1, 2]—that the absorbing medium has a rigid solid frame. This would normally be a good approximation over most of the frequency range of interest, provided the absorbent and structure were not in contact. Light contact would probably not violate the assumptions made here, but bonding between the absorbent and the plate would very likely necessitate the use of an absorbent model that took account of both structural vibration of the solid frame of the material and fluid/structural coupling. This would considerably complicate a predictive model for structural damping, and the essential simplicity of the infinite-plate approach would be lost.

ACKNOWLEDGMENT

Partial funding for the research reported in this paper was furnished by EPSCR grant GR/L52734, held jointly with Heriot-Watt University and the University of Nottingham.

REFERENCES

1. A. CUMMINGS, H. J. RICE and R. WILSON 1999 *Journal of Sound and Vibration* **221**, 143–167. Radiation damping in plates, induced by porous media.
2. R. J. M. CRAIK, D. TOMLINSON and R. WILSON 2000 *Proceedings of Acoustics* 2000 *Meeting, University of Liverpool*, 17–18 *April* 2000. Radiation into a porous medium.
3. M. E. DELANY and E. N. BAZLEY 1970 *Applied Acoustics* **3**, 105–116. Acoustical properties of fibrous absorbent materials.
4. F. P. MECHEL 1988 *Journal of the Acoustical Society of America* **83**, 1002–1013. Design charts for sound absorber layers.